Journal of Power Sources 196 (2011) 10074–10078

Contents lists available at SciVerse ScienceDirect

Journal of Power Sources

journal homepage: www.elsevier.com/locate/jpowsour

Short communication

Integrated thermal management strategy and materials for solid oxide fuel cells

Michael C. Tucker*, Lei Cheng

Environmental Energy Technology Division, Lawrence Berkeley National Laboratory, 1 Cyclotron Rd., Berkeley, CA 94720, United States

ARTICLE INFO

Article history:
Received 31 March 2011
Received in revised form 24 August 2011
Accepted 24 August 2011
Available online 31 August 2011

Keywords:
Thermal management
Hotspot
SOFC
Temperature distribution
PTC

ABSTRACT

The application of positive temperature coefficient (PTC) thermistors to thermal management of solid oxide fuel cells (SOFCs) is considered. A strategy is proposed for eliminating hotspots and reducing temperature gradients in SOFCs via inclusion of a material that exhibits a dramatic change in resistance near the desired maximum cell temperature. Three PTC thermistor materials with transition temperatures near the maximum desirable SOFC operating temperature are identified and screened for compatibility with common SOFC materials. All are found to be unsuitable because of reaction with the SOFC materials or unacceptably small PTC effect.

1. Introduction

Solid oxide fuel cells (SOFCs) contain multiple layers of various ceramic materials. These materials are generally chosen to display similar coefficients of thermal expansion (CTE), so as to minimize thermal stress upon temperature excursions [1]. SOFCs are also typically operated "isothermally", in the range 650–1000 °C. Although the nominal operation temperature is constant in time (after initial start-up transients), temperature may vary considerably across the area of the cell. This temperature variation arises from a number of factors, including variation in fuel concentration along the flow path, variation in current density (and therefore internal heat production) across the cell area, and edge effects pertaining to cooling at the perimeter of the stack [1–4]. Numerous efforts to model the temperature distribution in operating SOFCs have been reported [2–6]. Cross-cell thermal gradient predictions of >200 °C for tubular cells and >260 °C for planar cells have been reported [4,6]. Local thermal gradients can be so high, especially at the cell inlet, that authors use the term *hotspot* [2,4,5].

There are many reasons it is desirable to avoid hotspots and thermal gradients during SOFC operation, including: reduction of thermal stress so as to avoid brittle failure; homogenization of current distribution; reduction of maximum cell temperature to avoid degradation of cell and interconnect materials; and, simplification of operation models and control strategies. In this paper, we present a strategy for eliminating hotspots and reducing thermal gradients via inclusion of a material that exhibits a dramatic change in resistance near the desired maximum cell temperature.

2. Approach and background

Positive temperature coefficient (PTC) thermistor materials display a resistivity that increases abruptly upon increasing the temperature above the Curie temperature. The most well-known PTC materials are related to $BaTiO_3$, and display an increase in resistance of many orders of magnitude, with transition temperatures near room temperature [7]. They are used in thermostats and temperature-controlled heaters [8]. Fig. 1 shows some of the key elements of PTC thermistor behavior. At relatively low temperatures, the material displays a low resistivity, R_L. Upon heating above the transition temperature T_H, the resistivity increases dramatically to a higher value, R_H. Upon cooling below the transition temperature T_C, the resistivity recovers to R_L. There is generally some hysteresis between T_H and T_C.

We envision the use of PTC thermistors for managing thermal gradients and hotspots in fuel cells. The PTC material would be placed in the electrical path within a fuel cell stack. The PTC could be inserted as a contact layer between the cell and interconnect, as shown in Fig. 2, incorporated into one or both of the electrodes, or coated onto the interconnect. Should the local temperature exceed the PTC transition temperature, the resulting increase in local stack resistance would reduce or shut off local electrochemical activity. This would decrease the rate of local heating via ohmic and exothermic reaction mechanisms, causing the local temperature to decrease. Once the temperature decreased beyond the cooling

* Corresponding author. Tel.: +1 510 486 5304; fax: +1 510 486 4881.
E-mail address: mctucker@lbl.gov (M.C. Tucker).

0378-7753/$ – see front matter © 2011 Elsevier B.V. All rights reserved.
doi:10.1016/j.jpowsour.2011.08.100

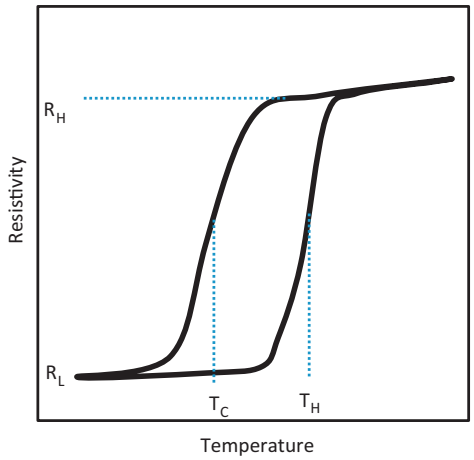

Fig. 1. Schematic representation of positive temperature coefficient (PTC) thermistor behavior. The resistivity increases abruptly above the transition temperature T_H. Hysteresis may be observed upon cooling.

transition point, the resistance of the PTC material would drop dramatically and normal electrochemical function would resume. By selecting the transition point of the PTC material, a maximum allowable local temperature within the stack could be set. Hysteresis between the heating and cooling transition points may be beneficial because the local temperature must be somewhat lower than the maximum allowable temperature before normal electrochemical function can resume.

Our approach is to identify suitable PTC thermistor candidate compositions, assess the magnitude of the PTC effect for bulk materials, and determine if the effect persists when the materials are applied as a thin layer on relevant SOFC materials including $(MnCo)_3O_4$-coated 441 stainless steel (MCO-441) and LSCF.

The PTC composition must fulfill the following requirements: compatibility with other cell materials; high electronic conductivity below the transition point; and low conductivity above the transition point. To guide our search for suitable materials, we can estimate the magnitude of the PTC transition needed to produce the desired effect. For example, we might want the PTC layer to contribute no more than an additional 10% to total impedance below the transition point, and to provide at least a doubling of the total impedance above the transition point. In this case an order of magnitude or more increase in the conductivity above the transition point would be required. The required thickness of the PTC layer would be determined by the relative values of the cell area-specific resistance (ASR) and PTC resistance.

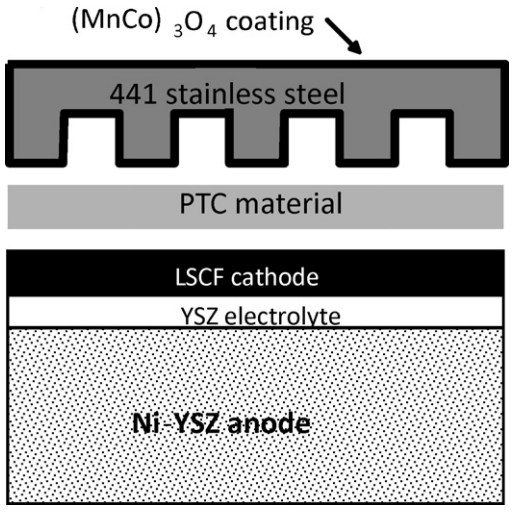

Fig. 2. Schematic representation of the placement of a PTC material in the electrical path of a SOFC stack.

A few examples of materials that display the PTC thermistor effect in the typical SOFC operating temperature range were identified from the literature. In this work, we explore the suitability of these three materials for application in SOFCs.

Manganese oxide (MNO) – PTC behavior has been reported to accompany the reversible conversion of α-Mn_2O_3 (low temperature) to tetragonal-Mn_3O_4 (high temperature) [9]. Upon increasing the temperature above 900 °C, the conductivity drops from 10 to 0.3 S cm^{-1}, and remains low until the temperature is reduced to 750 °C or lower.

$BaCo_{0.7}Fe_{0.3}O_{3-\delta}$ (BCF) – In the range 700–900 °C, BCF displays hexagonal perovskite structure, and conductivity of 20 S cm^{-1} [10]. Above 900 °C, the structure converts to cubic phase, and the conductivity drops to 6 S cm^{-1}. Cooling below 850 °C reverses the process.

$BaPbO_3$ (BPO) – PTC behavior has been observed for various compositions in the BPO family, including $Ba_{1-x}Sr_xPb_{1+y}O_3$ [11], $(Sr_{0.6}Ba_{0.4})_{1-x}(La, K)_xPbO_3$ [12], and $Sr_{0.7}Ba_{0.3}Pb_{1-x}Bi_xO_3$ [13]. The transition temperature and magnitude depend on the composition of the material, but in all cases the transition temperature is in the range 700–800 °C. $BaPb_{1.2}O_3$ displayed almost one order of magnitude decrease in the conductivity upon transition; this was among the largest transitions for this family of compositions [11].

3. Experimental methods

Materials. Powders of BCF and BPO were prepared by glycine–nitrate combustion synthesis, followed by calcining at 900 °C. MNO (Mn_2O_3) was purchased from Aldrich.

Resistivity. Powder of each composition was ball-milled with binder (PVB, DBT, MFO) in IPA, dried, sieved, pressed into pellets of approximately 1 cm diameter and 3 mm thick and sintered at 1050 °C (BPO and MNO) or 1200 °C (BCF) for 2 h in air. Pt mesh leads were applied to the pellets with Pt paste. Four-probe DC resistance and AC impedance measurements were taken at 600–950 °C in air using a potentiostat-galvanostat (Biologic VMP-3). BCF and BPO were observed to be hydroscopic, so these specimens were stored in a dessicator prior to testing.

XRD and SEM. XRD (Philips X'Pert) was used to confirm that the intended BCF and BPO phases were formed after calcining. The XRD traces were consistent with literature reports for these materials [10,13]. Cross-sections of tested specimens were imaged with SEM and EDS (Hitachi S4300SE/N).

ASR measurements. Specimens for ASR measurements were prepared by depositing inks of the PTC materials onto LSCF or coated stainless steel substrate coupons. Inks were prepared by mixing the powders with Ferro B75717 printing vehicle. 441 stainless steel coupons were coated with $Mn_{1.5}Co_{1.5}O_4$ (MCO) by screenprinting at Pacific Northwest National Laboratory (PNNL). LSCF coupons were prepared by ball-milling LSCF powder (Praxair) with binderspolyvinyl butyral, dibutyl phthalate, and Menhaden fish oil (PVB, DBT, MFO) in IPA. The powder was then dried, sieved, and pressed into coupons and sintered at 1200 °C for 2 h. LSCF ink was screen printed onto both sides of the coupon and sintered at 1050 °C for 2 h to produce a porous LSCF layer coating the dense LSCF coupon. PTC layers were then screen printed onto the MCO or porous LSCF layer, dried under a heat lamp and sintered in air at 1000 °C for 2 h. Pt paste (Heraeus CL11-5349) and Pt mesh (Alfa Aesar 10283) were applied as current collectors on the PTC layers, and sintered at 800 °C. Pt mesh was spot-welded to the 441 coupon. DC current was applied in a 4-probe configuration using a potentiostat

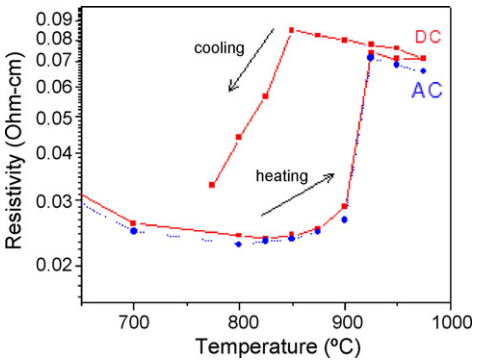

Fig. 3. Temperature-dependence of the resistivity of bulk BCF as determined with 4-probe AC impedance (blue) and DC polarization (red). (For interpretation of the references to color in this figure legend, the reader is referred to the web version of the article.)

(Biologic VMP3). ASR values for CCM/LSCF were divided by 2 to obtain the per-interface ASR reported in Section 4.

4. Results and discussion

4.1. BCF

The PTC effect was observed for a bulk pellet of BCF, as shown in Fig. 3. The DC conductivity and AC impedance measured during heating were quite similar, suggesting minimal ionic conduction. The value of the resistivity below 900 °C is consistent with the previous report by Kinoshita et al. [10]. Above 900 °C, the resistivity increased abruptly, but the magnitude of the increase was smaller than observed by Kinoshita et al. Upon cooling below 825 °C, the resistivity again decreased.

To mimic addition of BCF to a SOFC cathode, we prepared a dense LSCF coupon coated with a thin porous LSCF layer, and coated this with a thin layer of BCF. The area-specific resistance (ASR) of this specimen was recorded upon heating and cooling, as shown in Fig. 4. Note that the ASR expected for the dense LSCF substrate is three orders of magnitude less than the total ASR observed for the BCF-coated sample, suggesting the relatively low conductivity of the BCF layer dominates the total sample ASR. In contrast to the bulk BCF pellet, the desired PTC effect was not observed. In fact the ASR increased slightly during heating and continued to increase during cooling.

After resistivity testing, the BCF/LSCF sample was cross-section and analyzed with SEM/EDAX. Fig. 5 shows an image of the specimen, and an EDAX linescan across the interface between the porous and dense layers. There is no visual resolution between the porous BCF and porous LSCF layers. The concentration of La and Ba is also homogeneous across the interface (Fig. 5b), suggesting complete

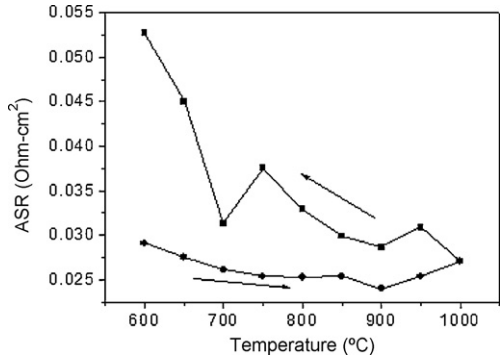

Fig. 4. Temperature-dependence of the ASR for BCF deposited on an LSCF substrate.

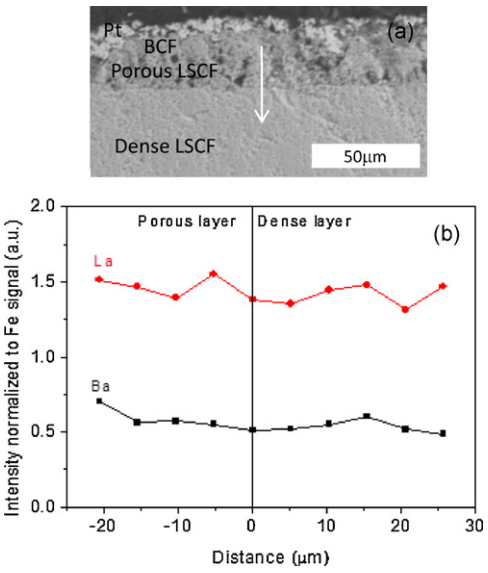

Fig. 5. Post-testing analysis of BCF deposited on an LSCF substrate. (a) SEM image of polished cross-section. The arrow indicates the EDAX linescan path. (b) EDAX linescan for La and Ba (both normalized to Fe signal intensity).

interdiffusion and reaction between LSCF and BCF. We surmise that the failure of the thin BCF layer to produce the desired PTC effect is due to this reaction with LSCF.

4.2. BPO

A bulk pellet of BPO was heated and cooled at 5 °C min^{-1} while recording conductivity as shown in Fig. 6a. No clear PTC effect was observed at this temperature ramp rate, however, the conductivity did return to its initial value after holding the sample at 650 °C

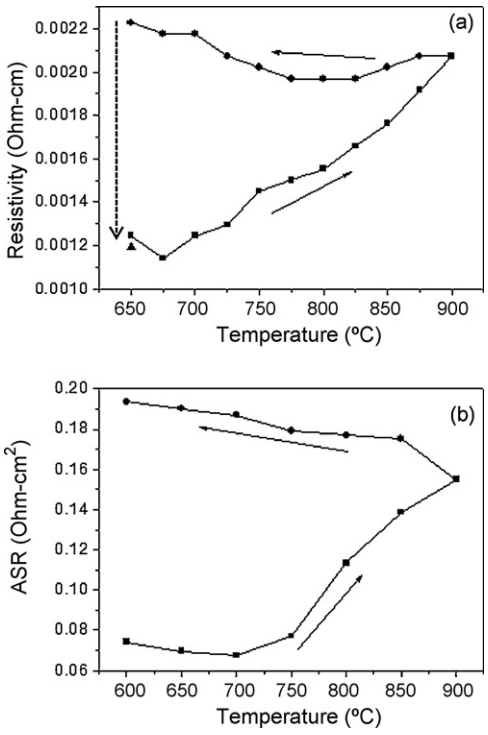

Fig. 6. BPO behavior. (a) Temperature-dependence of the resistivity of bulk BPO as determined with 4-probe DC polarization. (b)Temperature-dependence of the ASR for BPO deposited on an LSCF substrate.

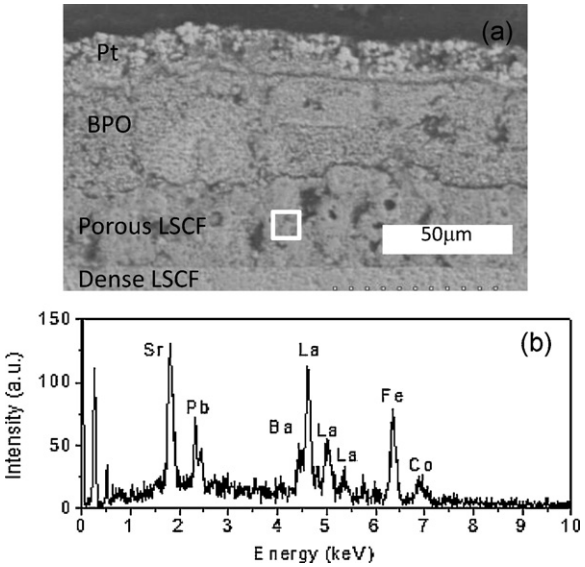

Fig. 7. Post-testing analysis of BPO deposited on an LSCF substrate. (a) SEM image of polished cross-section. (b) EDAX spectrum for the area of the LSCF layer indicated by the white box in (a). Note the presence of distinct peaks assigned to Ba and Pb.

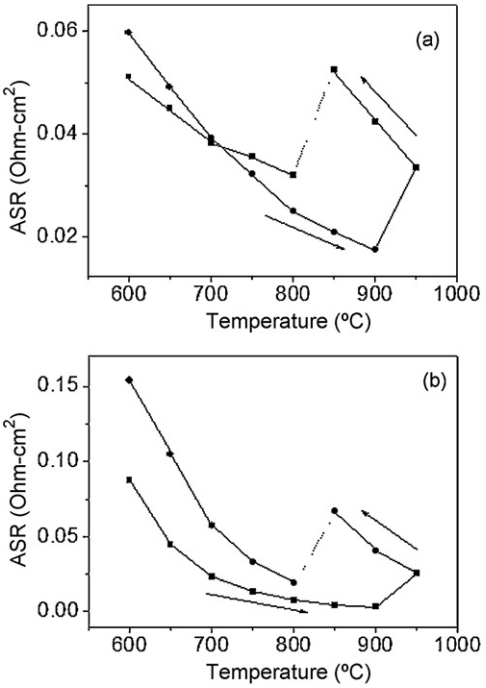

Fig. 8. Temperature-dependence of the ASR for MNO deposited on (a) LSCF substrate and (b) MCO-coated 441 stainless steel substrate.

overnight. We then prepared a thin BPO layer on porous/dense LSCF substrate. The conductivity of the specimen is shown in Fig. 6b. Like BCF above, the total ASR is dominated by the relatively low conductivity of BPO. The ASR increased moderately upon heating above 750 °C, but did not recover upon cooling. Analysis of the specimen after testing revealed delamination at the BPO/LSCF interface and some diffusion of Pb into LSCF (Fig. 7). These results were not promising enough to warrant further effort.

4.3. MNO

We attempted to observe the PTC effect for a bulk sample of MNO, but found that the conductivity took many hours to stabilize at each temperature point. The PTC effect for MNO accompanies oxidation of the Mn, so we considered that slow incorporation

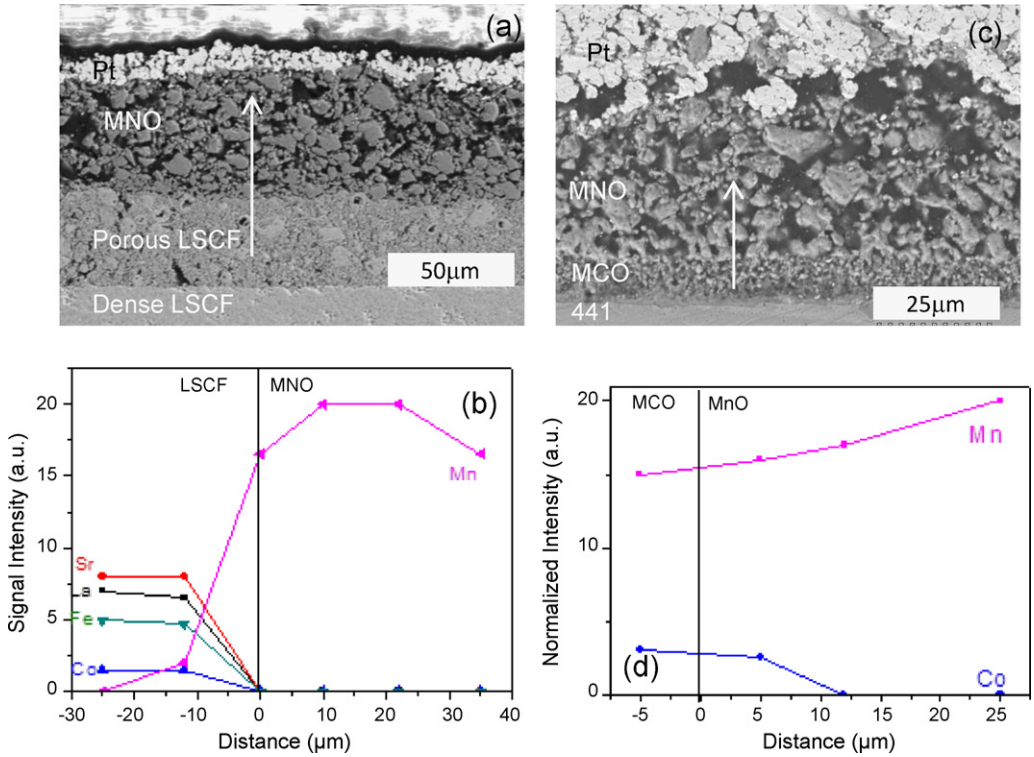

Fig. 9. Post-testing analysis of MNO deposited on (a and b) LSCF substrate and (c,d)MCO-coated 441 stainless steel substrate. (a and c) SEM images of polished cross-sections. The arrows indicate the EDAX linescan paths. (b and d) EDAX linescan across the LSCF/MNO and MCO/MNO interfaces.

of oxygen into the structure was causing the sluggish behavior. Expecting that a thin, porous layer of MNO might display faster transition, we prepared a MNO layer on LSCF and MCO-coated 441 steel substrates. The ASR for these specimens is shown in Fig. 8. The PTC effect was observed, although a long hold at 800 °C upon cooling was required to effect the transition. The ASR below the transition temperature is larger and more thermally activated than is desirable. Also, the magnitude of the PTC transition was too low to introduce a significant change in the total ASR of a SOFC stack incorporating a thin MNO layer. It is possible that optimization of the MNO microstructure, addition of dopants, or other manipulations might improve the PTC behavior. After testing, the specimens were cross-sectioned and analyzed with SEM/EDAX as shown in Fig. 9. Minimal interdiffusion was observed, suggesting that MNO does not react deleteriously with LSCF and MCO.

5. Conclusions

A strategy for thermal management of SOFCs utilizing positive-temperature-coefficient (PTC) thermistor materials is proposed. No suitable practical material was found, however the proposed strategy is expected to be effective should an appropriate material be identified. Three types of PTC material with resistivity transitions in the range of SOFC operating temperature were identified from the literature. We attempted to reproduce the reported PTC behavior with bulk specimens of each material, and then applied a thin layer of each material to LSCF coupons. Our observations lead us to conclude that each material is unsuitable as an aid in SOFC thermal management for the following reasons. BCF reacts completely with LSCF, and therefore does not retain PTC behavior when in contact with the cathode material. BPO did not display PTC behavior when in contact with LSCF, possibly due to slow transition kinetics or reaction with LSCF. MNO did produce PTC behavior on LSCF and MCO-coated 441 substrates. The magnitude of the transition was too small, however, and occurred very slowly. Modification of MNO, insertion of a barrier layer to prevent reaction, or identification of other candidate materials may be fruitful areas for further work.

Acknowledgements

This work was supported by the U.S. Department of Energy, National Energy Technology Laboratorty and in part by the U.S. Department of Energy under Contract No. DE-AC02-05CH11231. The authors thank Program Manager Joseph Stoffa, and Jeffry Stevensonand Ryan Scott at Pacific Northwest National Laboratory for MCO deposition.

References

[1] H. Apfel, M. Rzepka, H. Tu, U. Stimming, J. Power Sources 154 (2006) 370–378.
[2] Z. Qu, P.V. Aravind, S.Z. Boksteen, N.J.J. Dekker, A.H.H. Janssen, N. Woudstra, A.H.M. Verkooijen, Int. J. Hydrogen Energy 36 (16) (2011) 10209–10220.
[3] M. Iwata, T. Hikosaka, M. Morita, T. Iwanari, K. Ito, K. Onda, Y. Esaki, Y. Sakaki, S. Nagata, Solid State Ionics 132 (2000) 297–308.
[4] P.-W. Li, M.k. Chyu, J. Power Sources 124 (2003) 487–498.
[5] Y. Wang, F. Yoshiba, T. Watanabe, S. Weng, J. Power Sources 170 (2007) 101–110.
[6] K.P. Recknagle, R.E. Williford, L.A. Chick, D.R. Rector, M.A. Khaleel, J. Power Sources 113 (2003) 109–114.
[7] E. Andrich, Electron. Appl. 26 (1965).
[8] Z.C. Li, B. Bergman, Sens. Actuators A 118 (2005) 92–97.
[9] J.H. Kim, abd G.M. Choi, Solid State Ionics 130 (2000) 157–168.
[10] K. Kinoshita, H. Kusaba, G. Sakai, K. Shimanoe, N. Miura, N. Yamazoe, Chem. Lett. 41 (2002) 2–413.
[11] H. Nagamoto, H. Kagotani, T. Okubo, J. Am. Ceram. Soc. 76 (8) (1993) 2053–2058.
[12] M. Yasukawa, S. Itoh, T. Kono, J. Alloys Compd. 390 (2005) 250–254.
[13] M. Yasukawa, T. Kono, Solid State Commun. 146 (2008) 458–461.